J Solid State Electrochem (2011) 15:587–592
DOI 10.1007/s10008-010-1128-3

ORIGINAL PAPER

Meso-macroporous Co_3O_4 electrode prepared by polystyrene spheres and carbowax templates for supercapacitors

Yanhua Li · Kelong Huang · Suqin Liu · Zufu Yao · Shuxin Zhuang

Received: 27 January 2010 / Revised: 10 June 2010 / Accepted: 13 June 2010 / Published online: 27 June 2010

Abstract Meso-macroporous Co_3O_4 electrode is synthesized by drop coating with a mixed solution containing Co$(OH)_2$ colloid, polystyrene spheres, and carbowax (namely polyethylene glycol), followed by calcining at 400 °C to remove polystyrene spheres and carbowax. For comparison, nonporous Co_3O_4 and mesoporous Co_3O_4 electrodes are prepared by drop coating with $Co(OH)_2$ colloid and with a mixed solution containing $Co(OH)_2$ colloid and carbowax under the same condition, respectively. Capacitive property of these electrodes is measured by cyclic voltammetry, potentiometry and electrochemical impedance spectroscopy. The results show that meso-macroporous Co_3O_4 electrode exhibits larger specific capacitance than those of nonporous Co_3O_4 electrode and mesoporous Co_3O_4 electrode at various current densities. The specific capacitance of meso-macroporous Co_3O_4 electrode at the current density of 0.2 A g^{-1} is 453 F g^{-1}. Meanwhile, meso-macroporous Co_3O_4 electrode possesses the highest specific capacitance retention ratio at the current density ranging from 0.2 to 1.0 A g^{-1}, indicating that meso-macroporous Co_3O_4 electrode suits to high-rate charge–discharge.

Y. Li · K. Huang (✉) · S. Liu · Z. Yao · S. Zhuang
College of Chemistry and Chemical Engineering,
Central South University,
Changsha,
Hunan 410083, China
e-mail: klhuang@mail.csu.edu.cn

Y. Li
Department of Chemical Engineering
and Environmental Protection, Changsha Aeronautical Vocational
and Technical College,
Changsha,
Hunan 410124, China

Keywords Electrochemical capacitors · Porous tricobalt tetraoxide · Polystyrene spheres · Carbowax · Templates

Introduction

Electrochemical capacitors (supercapacitors) recognized as energy storage devices have attracted great attention due to their high power density, long cycle life, and short charge time. Carbon materials [1, 2], metal oxides [3–14], and conducting polymers [15, 16] are three major types of supercapacitor electrode materials. Carbon materials show limited energy capacity and power output, which hinders their practical application in some areas where high energy density is required. Short cycle life of conducting polymers limits their application in electrochemical capacitors. Among the metal oxides, RuO_2 exhibits high specific capacitance, but presents the drawbacks of lack of abundance and high cost. In order to reduce cost, efforts have been made to find other metal oxides with good electrochemical performance to replace RuO_2, e.g., cobalt oxide [6–8], nickel oxide [9–11], and manganese oxide [12–14]. Co_3O_4 materials are widely used in many fields, such as catalyst [17, 18], magnetic materials [19], lithium-ion batteries [20, 21], and field emission properties [22]. However, a few papers have been reported about Co_3O_4 for supercapacitor electrode materials. Cobalt oxide single electrode was fabricated by the sol-gel process [23]. The largest specific capacitance of cobalt oxide single electrode was 291 F g^{-1}. Co_3O_4 thin films were constructed by spray pyrolysis [7]. The specific capacitance of spray deposited Co_3O_4 thin film electrodes was 74 F g^{-1}. A radio frequency sputtering method was used to fabricate Co_3O_4-based thin films, and their capacitance depended on the sputtering gas ratio of $O_2/(Ar + O_2)$ [24].

In recent years, porous transition metal oxides have attracted widely attention due to their excellent supercapacitive performance [25]. Xue et al. [26] fabricated mesoporous MnO_2 electrochemical capacitor electrodes through triblock copolymer species as templates. Nakayama et al. [27] prepared the macroporous-layered manganese oxide electrochemical capacitor electrode, and the results showed that macroporous-layered manganese oxide electrode exhibited good pesudocapacitive behavior. All their work focused only on synthesizing single-sized pore supercapacitor electrode materials. Compared with single-sized pore materials, however, hierarchical porous materials containing both interconnected macroporous and mesoporous structures can enhance properties due to improved mass transport through the material and maintenance of a specific surface area on the level of fine pore [28, 29]. To date, there are few reports about meso-macroporous Co_3O_4 supercapacitor electrode material. Thus, it is very necessary to study meso-macroporous Co_3O_4 supercapacitor electrode material.

In the present work, meso-macroporous Co_3O_4 electrode was synthesized by drop coating with a mixed solution of $Co(OH)_2$ colloid, polystyrene spheres, and carbowax, then calcined at 400 °C. For comparison, nonporous Co_3O_4 and mesoporous Co_3O_4 electrodes were fabricated by drop coating with $Co(OH)_2$ colloid and with a mixed solution of $Co(OH)_2$ colloid and carbowax by the same manner, respectively. Electrochemical studies showed that meso-macroporous Co_3O_4 electrode material possessed good capacitive behavior.

Experimental

All reagents used in this experiment were of analytical grade without further purification. Polystyrene spheres (PS) with a diameter of 600 nm were acquired from Duke Scientific Corporation. A nonionic surfactant, carbowax 20000 (namely polyethylene glycol 20000), was purchased from Aldrich Chemicals. An indium-tin-oxide (ITO)-coated glass plate was used as the substrate.

A typical experiment procedure was shown as follows: $Co(OH)_2$ precipitate was synthesized by slowly adding LiOH solution into $CoSO_4$ solution with vigorous magnetic stirring under room temperature. When finished, the precipitate was filtered, and washed thoroughly with deionized water, then redispersed with glacial acetic acid. The obtained $Co(OH)_2$ colloidal solution was mixed with polystyrene spheres and carbowax. Finally, the above mixture was dropped onto ITO substrate and dried at room temperature, followed by calcining at 400 °C for 30 min in air to remove polystyrene spheres and carbowax. As a result, meso-macroporous Co_3O_4 electrode, denoted as PSC–Co_3O_4, was obtained. Non-porous Co_3O_4 electrode, referred to as N-Co_3O_4, was prepared onto ITO substrate by drop coating with $Co(OH)_2$ colloid under the same condition. Mesoporous Co_3O_4 electrode, designated as C–Co_3O_4, was synthesized by drop coating with a mixture of $Co(OH)_2$ colloid and carbowax by the same manner.

X-ray diffraction (XRD) pattern was recorded on a Rigaku D/max2550VB$^+$18kw with Cu Kα radiation. The size distribution and morphology of Co_3O_4 were observed by scanning electron microscopy (FEI, Sirion200). Electrochemical studies of the as-obtained electrodes were evaluated by cyclic voltammetry (CV), potentiometry, and electrochemical impedance spectroscopy using a CHI 660B electrochemical workstation (Shanghai, China) in a conventional three-electrode cell. The working electrodes with the geometric surface area of 1 cm^2 were the as-prepared Co_3O_4 electrode. A Pt plate and a saturated calomel electrode were used as the counter and reference electrodes, respectively. A 2-M KOH solution was used as the electrolyte. All the electrochemical measurements were carried out at room temperature. The impedance spectra were recorded by applying an AC voltage of 5-mV amplitude in the frequency range from 0.01 Hz to 100 kHz.

Results and discussion

X-ray diffraction analyses

Figure 1 displays XRD patterns of N–Co_3O_4 (a), C–Co_3O_4 (b), and PSC–Co_3O_4 (c). It can be observed that the positions of the characteristic peaks in three products are consistent. The peaks in curves a, b, and c are assigned to Co_3O_4 (JCPDS No. 43-1003) and ITO substrate. The peaks of ITO substrate are good agreement with that previously reported by Nakayama et al. [27]. No other peaks are observed in the XRD patterns except that peaks are attributed to Co_3O_4 and ITO. This suggests that carbowax and polystyrene spheres do not exist after calcining. Besides, carbowax and polystyrene spheres decompose fully under high temperature calcination according to relevant references [30–32]. Therefore, this is no evidence of residual carbowax and polystyrene spheres after calcining. The average crystallite sizes of N-Co_3O_4, C-Co_3O_4 and PSC–Co_3O_4 according to Scherrer formula are calculated to be about 9, 8, and 8 nm, respectively. There is only slight change in the average crystallite sizes of studied electrodes.

Morphology

SEM images of N–Co_3O_4 (a), C–Co_3O_4 (b), and PSC–Co_3O_4 (c) are shown in Fig. 2. As shown in Fig. 2a, there are no mesoporous and macroporous structures in N–

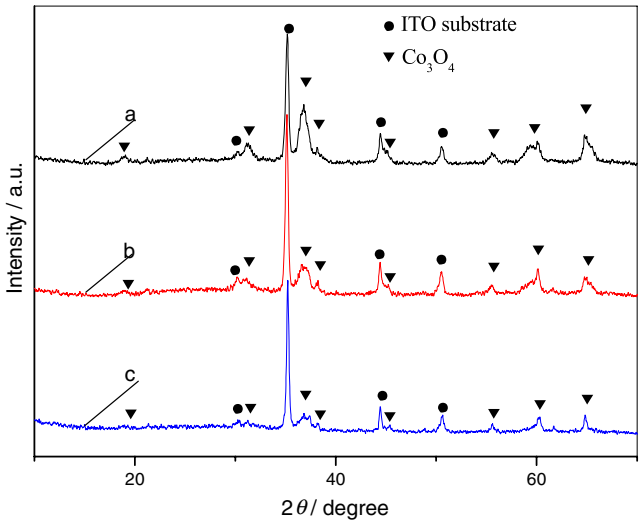

Fig. 1 XRD patterns of N–Co_3O_4 (**a**), C–Co_3O_4 (**b**), and PSC–Co_3O_4 (**c**)

Co_3O_4. However, as shown in Fig. 2b, mesopores below 15 nm is observed in C–Co_3O_4 due to removal of carbowax after calcining. Figure 2c displays mesoporous and interconnected macroporous structure in PSC–Co_3O_4 due to removal of carbowax and polystyrene spheres after calcining. The above mesoporous structure in C–Co_3O_4 and PSC–Co_3O_4 can be explained as the followings: Co^{2+} ion prefers to assemble around the carbon chains of carbowax via coordination with ether groups. The chemical interaction combined with the polymeric backbones provides a fixed template for the continual growth of mesoporous Co_3O_4 during the subsequent calcining process [8].

As for macroporous structure in PSC–Co_3O_4, polystyrene spheres are decomposed during calcining process. Macroporous structure of ca. 420 nm is obtained with 600 nm polystyrene spheres.

Electrochemical capacitor property

Figure 3 displays cyclic voltammograms of N–Co_3O_4, C–Co_3O_4, and PSC–Co_3O_4 in a 2-M KOH solution at a scan rate of 5 mV s^{-1}. The shape of CV curves reveals that the capacitance characteristic mainly results from the pseudocapacitive capacitance, which is caused by the fast and reversible faradaic redox reactions of electroactive material. A couple of redox peaks are observed within potential range from 0.25 to 0.46 V. The redox peaks correspond to the following electrode reaction.

$$Co_3O_4 + H_2O + OH^- \rightleftarrows 3CoOOH + e^- \quad (1)$$

Compared with N–Co_3O_4 and C–Co_3O_4, PSC–Co_3O_4 electrode exhibits the largest current density, indicating that PSC–Co_3O_4 electrode possesses the highest specific capacitance. This may be attributed to the improved mass transportation and electrode conduction [27], as a result of the mesopores and interconnected macropores in PSC–Co_3O_4 electrode.

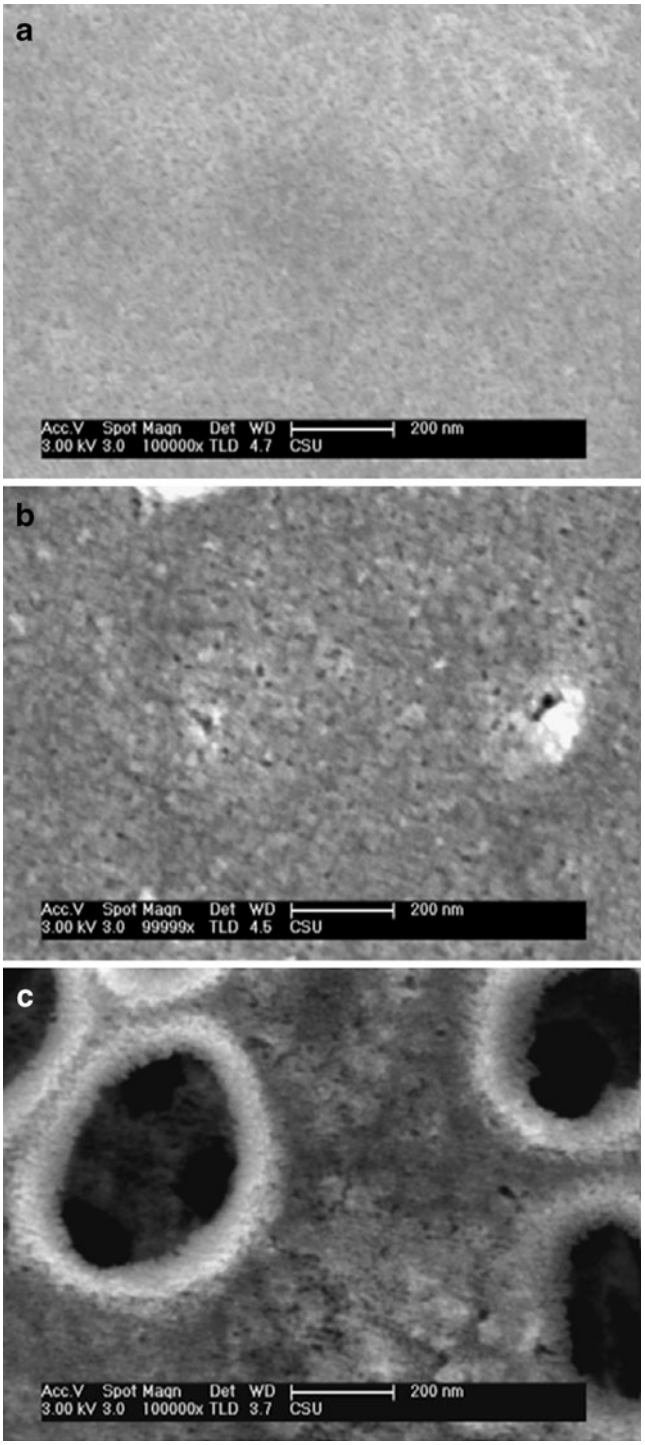

Fig. 2 SEM images of N–Co_3O_4 (**a**), C–Co_3O_4 (**b**), and PSC–Co_3O_4 (**c**)

Figure 4a shows cyclic voltammograms of PSC–Co_3O_4 in a 2-M KOH solution at scan rates of 5, 10, 20, 50, and

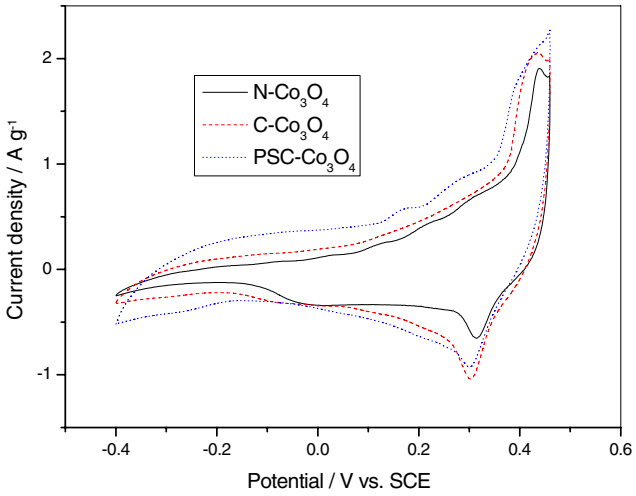

Fig. 3 Cyclic voltammograms of N–Co_3O_4, C–Co_3O_4, and PSC–Co_3O_4 in a 2-M KOH solution at a scan rate of 5 mV s^{-1}

100 mV s^{-1}. When increasing the scan rate, the anodic peak potential is shifted to higher value and that of the cathodic is shifted to lower value. The potential difference between the anodic and cathodic peak increases due to the polarization of electrode under high scan rate. Besides, the peak currents increase with the increase of the scan rate, indicating rapid reversible redox reaction occurred among the electrode materials. Figure 4b shows that the cathodic peak current (i_{pc}) is in proportion to the square root of the scan rate ($v^{1/2}$), indicating that the reaction kinetics is controlled by the diffusion process [33, 34].

In order to obtain information about capacitive property of N–Co_3O_4, C–Co_3O_4, and PSC-Co_3O_4 electrode materials, potentiometry was carried out in a 2-M KOH solution. Figure 5a shows constant current potentiometry curves of N–Co_3O_4, C–Co_3O_4, and PSC–Co_3O_4 electrode materials at the current density of 0.4 A g^{-1} in the potential range from 0 to 0.46 V. During the discharge steps, the capacitance of the working electrode within potential range of interest is related to the above indicated redox reaction (1), taking place at Co_3O_4 electrode/electrolyte interface. Therefore, the surface area of this interface is of crucial importance. The specific capacitance of the electrode can be calculated as follows

$$C_{sp} = \frac{I \times t}{V \times m} \tag{2}$$

where I is the discharge current, t is the discharge time, V is the potential range during discharge, m is the mass of active material in the electrode. According to the equation above, relationship between the specific capacitance (C_{sp}) from Eq. 2 and the current density (0.2, 0.3, 0.4, 0.5, 0.6, 0.8, and 1.0 A g^{-1}) is shown in Fig. 5b. As shown in Fig. 5b, PSC–Co_3O_4 electrode possesses larger specific capacitance than those of N–Co_3O_4 electrode and C–Co_3O_4 electrode at various current densities, in agreement with CV curves in Fig. 3. This is ascribable to the contributions from the surface of meso-macropores and interconnected macropores structure in PSC–Co_3O_4 electrode [35], which is desirable for the penetration of electrolytes and reactant into the whole electrode matrix [4]. The specific capacitance of PSC–Co_3O_4 electrode at the current density of 0.2 A g^{-1} is 453 F g^{-1}, which is much higher than CoOx materials prepared by Lin et al. (a maximum capacitance of 291 F g^{-1}) [23] and spray deposited Co_3O_4 film electrode (74 F g^{-1}) [7], despite

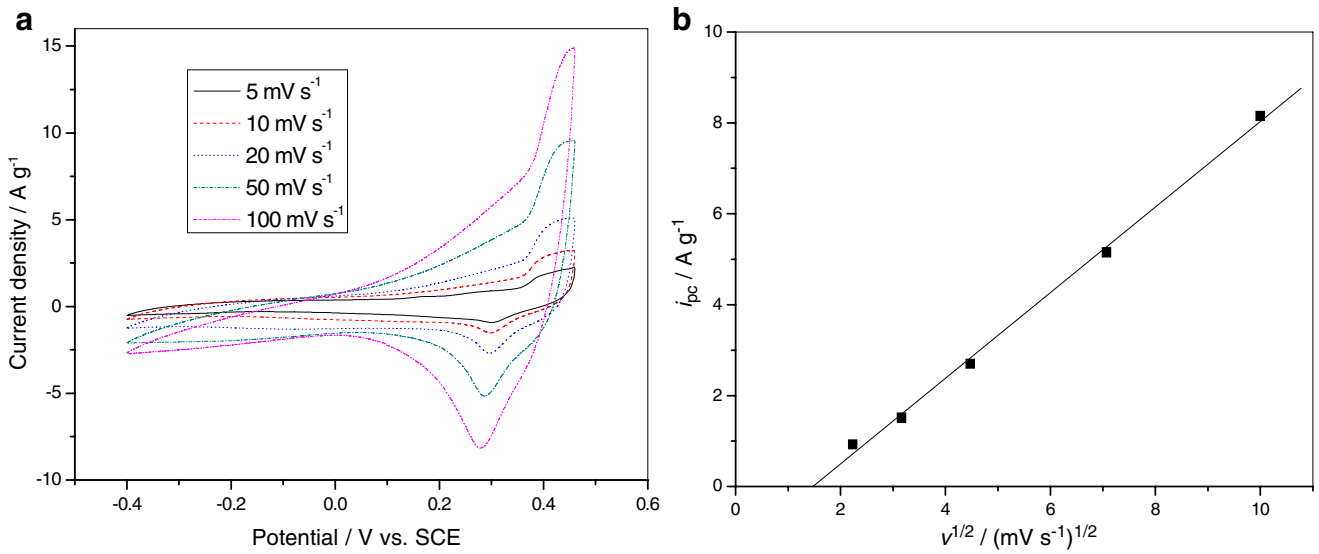

Fig. 4 Cyclic voltammograms of PSC–Co_3O_4 in a 2-M KOH solution at scan rates of 5, 10, 20, 50, and 100 mV s^{-1} (**a**); relationship between the cathodic peak current (i_{pc}) and the square root of the scan rate ($v^{1/2}$) (**b**)

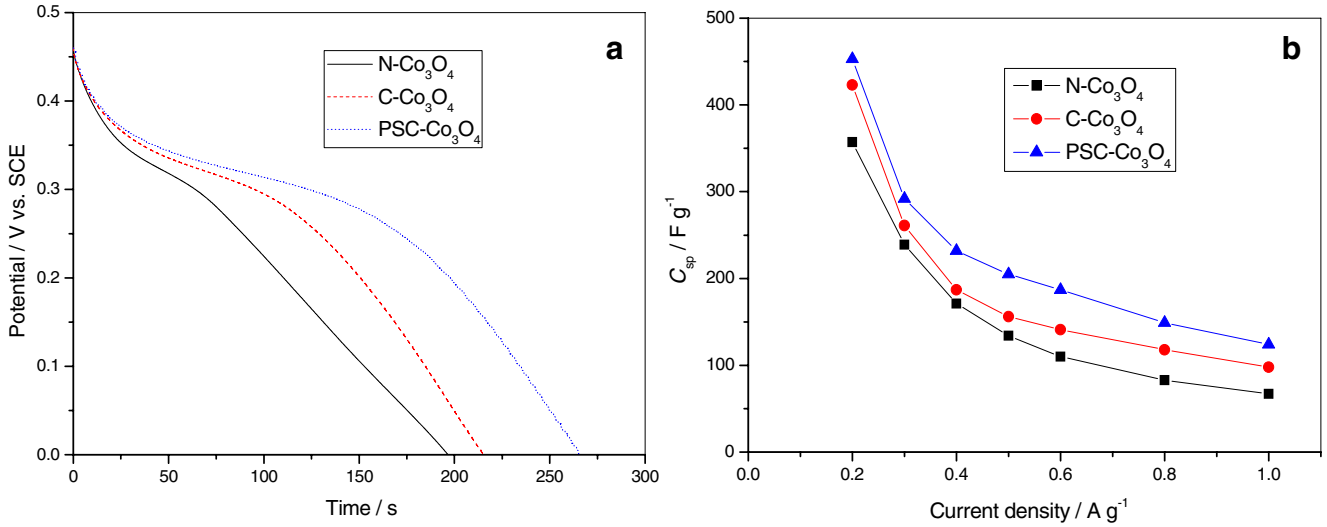

Fig. 5 Constant current potentiometry curves of N–Co_3O_4, C–Co_3O_4, and PSC–Co_3O_4 in a 2-M KOH solution at the current density of 0.4 A g^{-1} (**a**); relationship between the specific capacitance and the current density of N–Co_3O_4, C–Co_3O_4, and PSC–Co_3O_4 (**b**)

the less conductive property of ITO substrate. The specific capacitance can be increased significantly by the use of highly conductive substrate [27]. Meanwhile, this value is comparable with that obtained from mesoporous MnO_2 (a maximum capacitance of 449 F g^{-1}) [26], but much higher than that obtained from macroporous MnO_2 film at the slow scan rates (152–163.4 F g^{-1}) [27]. When the current density increases to 1.0 A g^{-1}, the specific capacitance retention ratios of N–Co_3O_4, C–Co_3O_4, and PSC-Co_3O_4 are 18.8%, 23.4%, and 26.3%, respectively, indicating that PSC–Co_3O_4 electrode suits to high-rate charge–discharge. The above results can be explained as the followings: the improved mass transportation and electrode conduction in PSC–Co_3O_4 electrode contribute to the high-rate performance.

Electrochemical impedance spectroscopy test was performed to further test the fundamental behavior of electrode materials for supercapacitors. Figure 6a presents measured and simulated Nyquist impedance plots for N–Co_3O_4, C–Co_3O_4, and PSC–Co_3O_4 electrodes measured at −0.3 V in a 2-M KOH solution in the frequency range $0.01 \sim 10^5$Hz. A corresponding equivalent circuit for modeling the measured impedance spectroscopy is shown in Fig. 6b. As shown in Fig. 6a, simulated Nyquist impedance plots match well with measured Nyquist impedance plots. In the high frequency range, the intercept at real part (Z') is a combinational resistance of ionic resistance of electrolyte, intrinsic resistance of substrate, and contact resistance between the active material and the current collector (R_e) [36]. The above combinational resistance is about 2 Ω cm^2, which is the same for all the electrodes. A depressed semicircle is observed in the high frequency region, which results from a parallel combination of the charge-transfer resistance (R_{ct}) caused by faradaic reactions and a constant phase element one (CPE_1). The calculated charge-transfer resistance for N-Co_3O_4, C–Co_3O_4, and PSC–Co_3O_4 electrode are 260, 214, and 82 Ω cm^2, respectively. The lower the charge-transfer resistance, the higher the specific capacitance of the electrode. PSC–Co_3O_4 electrode shows the lowest charge-transfer resistance, indicating that PSC–Co_3O_4 electrode possesses the highest specific capacitance, which is agreement with previous specific

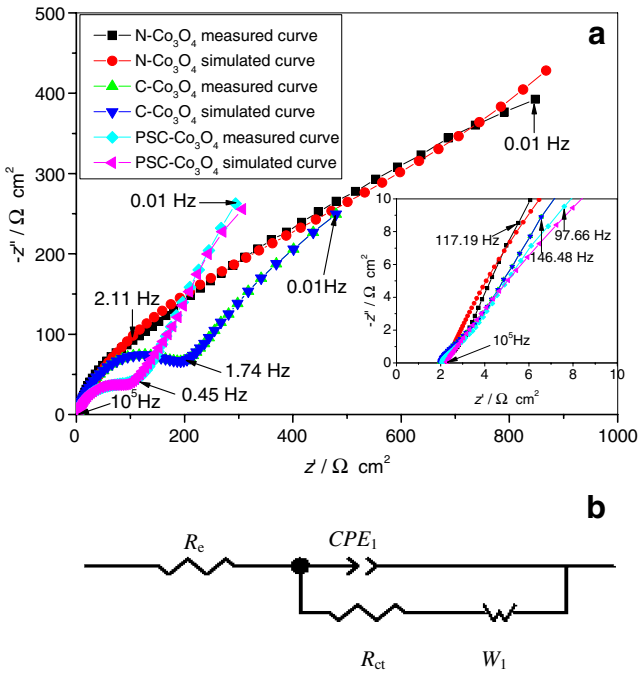

Fig. 6 Measured and simulated Nyquist impedance plots of N–Co_3O_4, C–Co_3O_4, and PSC–Co_3O_4 measured at −0.3 V (**a**); a corresponding equivalent circuit for modeling the measured impedance spectroscopy (**b**)

capacitance calculated by constant current potentiometry curve. Charge-transfer resistance is normally related to the electroactive surface area. In the low frequency range, the straight sloping line represents the electrolyte diffusion process (W_1) and the diffusion of OH^- ion in host materials. The slope of straight line increases in the order of N–Co_3O_4, C–Co_3O_4, and PSC–Co_3O_4 electrodes. Normally, a higher slope for the impedance line means a lower diffusive resistance for the electrolyte in the electrode by the shortened diffusion path of OH^- ion [36, 37]. In other words, PSC–Co_3O_4 electrode shows the lowest diffusive resistance for the electrolyte. This can be explained as the followings: macropores and mesopores in PSC–Co_3O_4 electrode can enhance the diffusivity of electrolyte ions in the pores.

Conclusions

Meso-macroporous Co_3O_4 electrode was prepared on indium tin oxide substrate using polystyrene spheres and carbowax as templates. For comparison, non-porous Co_3O_4 and mesoporous Co_3O_4 electrodes were synthesized on indium tin oxide without a template and with carbowax template, respectively. The result shows that meso-macroporous Co_3O_4 electrode exhibits the largest specific capacitance, as a result of the contributions from the surface of mesopores and interconnected macropores structure in meso-macroporous Co_3O_4 electrode. Meso-macroporous Co_3O_4 electrode reaches a maxium value of 453 F g^{-1} at the current density of 0.2 A g^{-1}. Moreover, the highest specific capacitance retention ratio is obtained in meso-macroporous Co_3O_4 electrode at the current density ranging from 0.2 to 1.0 A g^{-1}, indicating that meso-macroporous Co_3O_4 electrode suits to high-rate charge–discharge. In conclusion, high specific capacitance and specific capacitance retention ratio promote meso-macroporous Co_3O_4 as a novel electrode material in electrochemical capacitors. Further, this study provides a simple and available method to prepare other meso-macroporous transition metal oxides in electrochemical capacitors.

Acknowledgements This work is supported financially by National Natural Science Foundation of China (No. 50972165), Nonferrous Metal Research Fund of Hunan Provincial Nonferrous Group (No. Y 2008-01-007) and Scientific Research Fund of Hunan Provincial Education Department (No. 09C1055).

References

1. Centeno TA, Stoeckli F (2006) Electrochim Acta 52:560
2. Wu FC, Tseng RL, Hu CC, Wang CC (2004) J Power Sources 138:351
3. Subramanian V, Hall SC, Smith PH, Rambabu B (2004) Solid State Ionics 175:511
4. Hu CC, Chang KH, Lin MC, Wu YT (2006) Nano Lett 6:2690
5. Mondal SK, Munichandraiah N (2008) J Power Sources 175:657
6. Švegl F, Orel B, Hutchins MG, Kalcher K (1996) J Electrochem Soc 143:1532
7. Shinde VR, Mahadik SB, Gujar TP, Lokhande CD (2006) Appl Surf Sci 252:7487
8. Cao L, Lu M, Li HL (2005) J Electrochem Soc 152:A871
9. Wang YG, Xia YY (2006) Electrochim Acta 51:3223
10. Cheng J, Cao GP, Yang YS (2006) J Power Sources 159:734
11. Nathan T, Aziz A, Noor AF, Prabaharan SRS (2008) J Solid State Electrochem 12:1003
12. Subramanian V, Zhu H, Wei B (2006) J Power Sources 159:361
13. Yang XH, Wang YG, Xiong HM, Xia YY (2007) Electrochim Acta 53:752
14. Huang Q, Wang X, Li J (2006) Electrochim Acta 52:1758
15. Mastragostino M, Arbizzani C, Soavi F (2002) Solid State Ionics 148:493
16. Soudan P, Ho HA, Breau L, Belanger D (2001) J Electrochem Soc 148:A775
17. Fujita S, Suzuki K, Mori T (2003) Catal Lett 86:139
18. Tüysüz H, Comotti M, Schüth F (2008) Chem Commun 4022
19. Shen XP, Miao HJ, Zhao H, Xu Z (2008) Appl Phys A 91:47
20. Li YG, Tan B, Wu YY (2008) Nano Lett 8:265
21. Chou SL, Wang JZ, Liu HK, Dou SX (2008) J Power Sources 182:359
22. Varghese B, Hoong TC, Yanwu Z, Reddy MV, Chowdari BVR, Wee ATS, Vincent TBC, Lim CT, Sow CH (2007) Adv Funct Mater 17:1932
23. Lin C, Ritter JA, Popov BN (1998) J Electrochem Soc 145:4097
24. Kim HK, Seong TY, Lim JH, Cho WI, Yoon YS (2001) J Power Sources 102:167
25. Liu Y, Zhao W, Zhang X (2008) Electrochim Acta 53:3296
26. Xue T, Xu CL, Zhao DD, Li XH, Li HL (2007) J Power Sources 164:953
27. Nakayama M, Kanaya T, Inoue R (2007) Electrochem Commun 9:1154
28. Zhao Y, Zheng MB, Cao JM, Ke XF, Liu JS, Chen YP, Tao J (2008) Mater Lett 62:548
29. Yuan ZY, Su BL (2006) J Mater Chem 16:663
30. Pichot F, Pitts JR, Gregg BA (2000) Langmuir 16:5626
31. Yan H, Blanford CF, Holland BT, Parent M, Smyrl WH, Stein A (1999) Adv Mater 11:1003
32. Zampori L, Stampino PG, Cristiani C, Dotelli G, Cazzola P (2010) Appl Clay Sci 48:97
33. Singh RN, Koenig JF, Poillerat G, Chartier P (1990) J Electrochem Soc 137:1408
34. Scavetta E, Ballarin B, Gazzano M, Tonelli D (2009) Electrochim Acta 54:1027
35. Moriguchi I, Nakahara F, Furukawa H, Yamada H, Kudo T (2004) Electrochem Solid St 7:A221
36. Wu MS, Hsieh HH (2008) Electrochim Acta 53:3427
37. Wei WF, Cui XW, Chen WX, Ivey DG (2009) J Power Sources 186:543